Simulating the Nonlinear Klein-Gordon-Maxwell System in the Relativistic Limit with Mimetic Differences

Hayden Frye and Miguel A. Dumett

July 19, 2023

Publication Number: CSRCR2023-04

Computational Science & Engineering Faculty and Students Research Articles

Database Powered by the Computational Science Research Center Computing Group & Visualization Lab

COMPUTATIONAL SCIENCE & ENGINEERING

SAN DIEGO STATE UNIVERSITY

Computational Science Research Center
College of Sciences
5500 Campanile Drive
San Diego, CA 92182-1245
(619) 594-3430

Simulating the Nonlinear Klein-Gordon-Maxwell System in the Relativistic Limit with Mimetic Differences

Hayden Frye *and Miguel A. Dumett ‡

July 19, 2023

Abstract

This paper simulates, utilizing mimetic differences, the nonlinear interactions between circularly polarized electromagnetic waves (CPEMs) and a plasma in the quantum regime.

1 Introduction

The nonlinear Klein-Gordon-Maxwell (KGM) system of equations is particularly useful in modeling the interactions between a new class of an X-ray free electron laser and solid density plasmas. The model also has use in astrophysics with describing the EM wave-plasma interaction with X-rays and γ-rays produced by white dwarf cores and neutron stars. The goal is to simulate the plasma wake-field generation which is a phenomenon studied in designing next generation plasma/particle accelerators with applications in high energy physics experiments, and the medical and industrial fields.

1.1 Governing equations

The full KGM system of equations is described in [3] by

$$\partial_{tt}\psi + 2i\phi\partial_t\psi - \nabla^2\psi + 2ic\mathbf{A}\cdot\nabla\psi + (c^4 - \phi^2 + i\partial_t\phi + |\mathbf{A}|^2)\psi = 0 \tag{1}$$

$$\partial_{tt}\mathbf{A} - c^2\nabla^2\mathbf{A} - c\mathcal{P}_{df}[\mathbf{J}[\psi,\mathbf{A}]] = 0 \tag{2}$$

$$\nabla^2\phi = -\rho[\psi,\phi] \tag{3}$$

where $\mathcal{P}_{df}$ is the projection operator onto the divergence-free field as a result of the coulomb gauge constraint $\nabla\cdot\mathbf{A} = 0$.

The solutions are defined in $\psi\in\mathbb{C}$ and $(\phi,\mathbf{A})^T\in\mathbb{R}^{1+d}$ while the variables ρ and $\mathbf{J}$ are given by

$$\rho[\psi,\phi] = -Re(i\frac{\psi}{c}\cdot\overline{\partial_t^{[\phi]}\psi}) = -\frac{1}{c^2}(Re(i\psi\overline{\partial_t\psi}) + \phi|\psi|^2) \tag{4}$$

$$\mathbf{J}[\psi,\phi] = Re(i\psi\cdot\overline{\nabla^{[\mathbf{A}]}\psi}) = Re(i\psi\overline{\nabla\psi}) - \frac{\mathbf{A}}{c}|\psi|^2 \tag{5}$$

which both obey the continuity equation by way of conservation of charge and current respectively.

The system of equations (1)-(3) is considered relativistic as $c = 1$ and non-relativistic as $c \gg 1$ where the solutions become highly oscillatory and require a special numerical treatment via Gautchi-type exponential integrators with severely restricted time step requirements (CFL conditions) [4].

There have also been more recent efforts with constructing a 'twisted variables' numerical scheme for uniformly accurate time integration which involves recasting equation (1) as two equations with first-order time derivatives. Afterwards, the vector of the two solutions are then multiplied by a phase factor dependant on the constant c [3].

The physical system studied here is in [2], where the KGM system of equations is used to describe the relativistic interactions between plasma and attosecond laser pulses in the quantum regime. Specifically, the KGM system of equations is solved for a pseudo-distribution function describing an electron ensemble

*Computational Science Master Program at San Diego State University (hfrye1604@sdsu.edu).
†Jose E. Castillo, Editor
‡Computational Science Research Center at San Diego State University (mdumett@sdsu.edu).

in sufficiently dense plasmas [2]. In their numerical study, they specify a periodic simulation box with a constant charge and for a CPEM pump wave

$$i\partial_t \phi \longrightarrow 0 \tag{6}$$

$$2ic\mathbf{A} \cdot \nabla\psi \longrightarrow 0 \tag{7}$$

This gives us the set of equations (1)-(3) as

$$\partial_{tt}\psi = \nabla^2\psi - (c^4 - \phi^2 + |\mathbf{A}|^2)\psi - 2i\phi\partial_t\psi \tag{8}$$

$$\partial_{tt}\mathbf{A} = c^2\nabla^2\mathbf{A} - \frac{|\psi|^2}{c}\mathbf{A} \tag{9}$$

$$\nabla^2\phi = -\frac{1}{c^2}[i(\psi^*\partial_t\psi - \psi\partial_t\psi^*) + \phi|\psi|^2] \tag{10}$$

The initial conditions studied involve a slab of constant density plasma $\psi_0 = \sqrt{n_o}$ with the initial conditions of two CPEM pulse waves starting symmetrically on the both sides of the periodic simulation box,

$$\mathbf{A}(t=0) = A_0(z)[\hat{\mathbf{x}}cos(k_0 z) - \hat{\mathbf{y}}sin(k_0 z)]$$

where the envelope is $A_0(z) = e^{-(z\pm 25)^2}$.

1.2 Numerical Scheme

[2] solves the scheme for one dimension using a fourth-order Runge-Kutta method. This seems to be the reason for the formulation of the four equations in the original paper, where the first equation serves as a derivative function to help solve the system. Solving the system the same way in two or higher dimensions likely would not be doable however with the same Runge-Kutta scheme. Through the use of a two-dimensional mimetic Laplacian operator, solving the system for two dimensions with fourth-order Runge-Kutta is once again easily attainable.

Mimetic operators 'mimic' the properties of differential operators in vector calculus on a discrete grid. They obey conservation laws and other vector differential identities [1]. Matrix $\mathbf{L}$ is a discrete representation of ∇^2 such that when applied to a discrete vector u on a grid linearly approximates the vector $\mathbf{L}u = u''$. This allows the manipulation of differential equations using matrix algebra that could not be done otherwise.

Equations (8) and (9) can be solved with Runge-Kutta using the following substitutions:

$$\begin{gathered} U = U_1 \\ \tfrac{dU_1}{dt} = U_2 \\ \tfrac{dU_2}{dt} = \alpha\mathbf{L}U_1 + \beta U_1 + \gamma U_2 \end{gathered} \tag{11}$$

which with the mimetic Laplacian $\mathbf{L}$, can be rearranged in the form,

$$\frac{d}{dt}\begin{bmatrix} U_1 \\ U_2 \end{bmatrix} = \begin{bmatrix} 0 & \mathbf{I} \\ \alpha\mathbf{L} + \beta\mathbf{I} & \gamma\mathbf{I} \end{bmatrix}\begin{bmatrix} U_1 \\ U_2 \end{bmatrix} + Q = \mathbf{F}(U_1, U_2) \tag{12}$$

This form uses a sparse super matrix which for a mimetic Laplacian operator size of m by n, is $2m \times 2n$. Vector U stands for both ψ or $\mathbf{A}$ for a given α, β, and γ from their respective equations. Q is a source term that for both equations is zero but could potentially be used for verifying the scheme through the use of manufactured methods of solutions. $\mathbf{L}$ is the same for each equation since both solutions are defined on the same lattice. The fourth-order Runge-Kutta scheme therefore can be defined simply for each wave equation for the full solution vector $U_{12} = (U_1, U_2)^T$ as follows,

$$\begin{gathered} \mathbf{K}_1 = \mathbf{F}(U_{12}) \\ \mathbf{K}_2 = \mathbf{F}(U_{12} + \tfrac{\Delta t}{2}\mathbf{K}_1) \\ \mathbf{K}_3 = \mathbf{F}(U_{12} + \tfrac{\Delta t}{2}\mathbf{K}_2) \\ \mathbf{K}_2 = \mathbf{F}(U_{12} + \Delta t\mathbf{K}_3) \\ U_{12}^{n+1} = U_{12}^n + \tfrac{\Delta x}{6}(\mathbf{K}_1 + 2\mathbf{K}_2 + 2\mathbf{K}_3 + \mathbf{K}_4) \end{gathered} \tag{13}$$

Parameters α, β, and γ for each equation are shown in Table 1. It should be noted that some of the parameters contain the coupled solutions and need to be continually updated at each time step.

	ψ	$\mathbf{A}$
α	1	c^2
β	$-(c^4 - \phi^2 + \lvert\mathbf{A}\rvert^2)$	$-\frac{\lvert\psi\rvert^2}{c}$
γ	$-2i\phi$	0

Table 1: Coefficient parameters for super matrix in the Runge-Kutta fourth-order scheme

Equation (10) will need to be solved differently as it is a Poisson equation as opposed to a wave type equation. Luckily, the solution should be easily solved via the mimetic operator $\mathbf{L}$ as a linear system of equations $A\mathbf{x} = \mathbf{b}$ where the matrix A is built with the Laplacian $\mathbf{L}$ as

$$A = c^2\mathbf{L} - |\psi_1|^2\mathbf{I}. \tag{14}$$

For the right hand side, $\mathbf{b}$, we have

$$\mathbf{b} = i(\psi_1^*\psi_2 - \psi_1\psi_2^*) + \phi|\psi|^2 \tag{15}$$

Here ψ_1 is the original solution for equation (8) and ψ_2 is the first time derivative of the solution according to the scheme.

1.3 Boundary Conditions

Generally periodic boundary conditions are described on a torus of dimension d, $(x, z) \in \mathbb{T}^d$ [3]. Eliasson and Shukla describe solving the system of equations in a one dimensional periodic simulation box [2]. For the problem of a two-dimensional simulation box, the periodic boundaries can be specified for a vector of solutions $(\psi, \phi, \mathbf{A})^T$,

$$\begin{aligned}
(\psi_1, \phi, \mathbf{A}_1)^T|_{-L_x} &= (\psi_1, \phi, \mathbf{A}_1)^T|_{L_x} \\
(\psi_1, \phi, \mathbf{A}_1)^T|_{-L_y} &= (\psi_1, \phi, \mathbf{A}_1)^T|_{L_y} \\
(\psi_2, \mathbf{A}_2)^T|_{-L_x} &= (\psi_2, \mathbf{A}_2)^T|_{L_x} \\
(\psi_2, \mathbf{A}_2)^T|_{-L_y} &= (\psi_2, \mathbf{A}_2)^T|_{L_y}
\end{aligned} \tag{16}$$

Imposing periodic boundary conditions can most simply be done by altering the Laplacian $\mathbf{L}$ to ensure the solutions at the boundaries appear at the other end. The way this was achieved is by starting with the one-dimensional gradient and divergence operators. In both dimensions one-dimensional mimetic divergence operators $\mathbf{D}_x$ and $\mathbf{D}_y$ are defined using the parameters from the problem and modifying them to include terms on the top and bottom rows. Specifically, it has been inserted $1/2\Delta x$ on the second column on the top and bottom rows and $-1/2\Delta x$ on the second to last column top and bottom rows. This procedure was done for the divergence operators in both dimensions. This was taken from a Matlab example solution to a one-dimensional advection equation on a periodic boundary [1]. For the one-dimensional gradient operators $\mathbf{G}_x$ and $\mathbf{G}_y$, the top and bottom rows, are reversed and subtracted them onto themselves in a similar fashion to the divergences. Then the respective two-dimensional operators $\mathbf{G}_{xy}$ and $\mathbf{D}_{xy}$ are computed using the steps laid out in [1]. By multiplying them together the two-dimensional Laplacian operator $\mathbf{L}_{xy} = \mathbf{D}_{xy}\mathbf{G}_{xy}$ is obtained and successfully satisfy periodic boundary conditions for the solutions and their derivatives.

The periodic Laplacian does need to be conditioned however, due to a very high condition number, which is usually infinite to working precision. This initially posed a problem to solving the system as the Poisson equation needs the inverse of the operator. This issue seemed to be remedied by a simple preconditioning procedure multiplying the diagonal of the operator matrix by a factor of $\frac{1}{\Delta x^2}$, effectively bringing the condition number from infinite to working precision to double digits for 100×100 grid points. It was found that for different numbers of grid points the usefulness of this factor does not hold. Particularly, it was found that the diagonal scaling factor is sensitive to the number of grid points and might have some 'sweet spots' at smaller factors (see Figure 1). Figure 2 shows the resulting condition number related to the diagonal factor for 100 by 100 grid points.

2 Initial Results

I have initially had some trouble calculating the scalar potential ϕ due to the Laplacian operator turning out to be singular to working precision according to Matlab. As mentioned in the previous section, results are obtained by scaling the diagonal by a small enough factor that turns out some results without drastically changing the other two solutions within a small enough time frame.

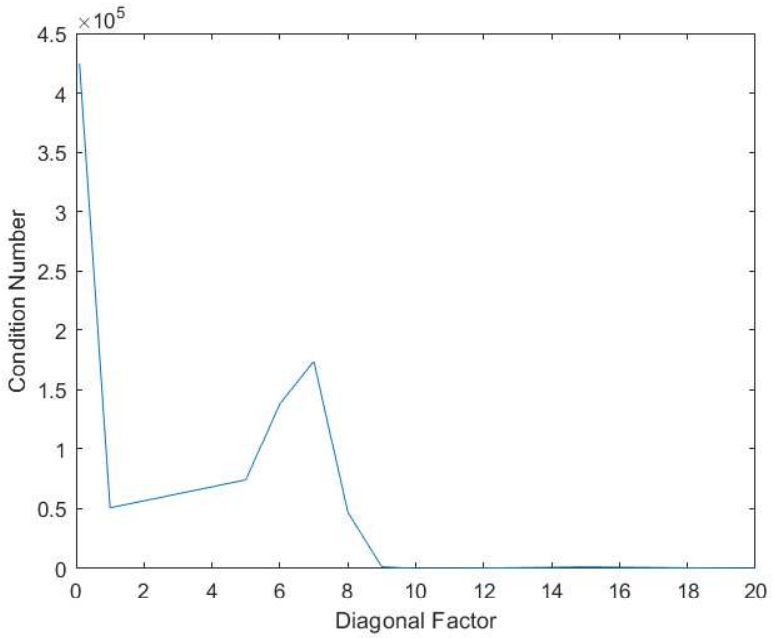

Figure 1: Condition number of the periodic Laplacian operator matrix with respect to the simple diagonal scaling factor for a 100 by 100 grid.

Another point of contention is the drastic differences in the sizes of constants. Some were in the ranges of $10^{25} - 10^{45}$ while others were in the ranges of $10^{-14} - 10^{-26}$. These differences made things very difficult keeping the computation stable as the computation would break down very quickly. Constants were simplified for the sake of being able to do more with evolving the equations and observing the trends between the physical quantities as opposed to the exact numbers associated.

A few interesting things occur as the equations evolve in time. An equal number of 100 cells were used in each dimension for the simulation with a time step using the CFL condition for stability. The system starts off with the time steps before the CPEM wave reaches the distribution. The particle distribution oscillates with its own charge distribution as well as diffuse on its own over the grid space. The results for an early time, before contact with the CPEM wave are exhibited in Figure 3.

As time steps advance, there is an interplay between the scalar potential and the particle distribution where they almost dance around each other as the particles disburse. As time progresses and the particle distribution continues to dissipate, saddle points in the scalar potential begin to form, as displayed in Figure 4 and Figure 5 where the distribution seems to stabilize.

As time progresses and the vector potential moves closer, the particle distribution begins to pitch and we begin to see a spike in momentum as mentioned in [2] with wake-field acceleration. This can be observed in Figure 6.

The particle velocity increases more than a factor of eight in magnitude before decreasing once again. Figure 6 shows the particle velocity around its maximum in time.

References

[1] Johnny Corbino and Jose Castillo. High-order mimetic finite-difference operators satisfying the extended gauss divergence theorem. *Journal of Computational and Applied Mathematics*, 364, 01 2020.

[2] Bengt Eliasson and P. K. Shukla. Relativistic laser-plasma interactions in the quantum regime. *Physical Review E*, 83(4), apr 2011.

[3] Patrick Krämer. *Numerical Integrators for Maxwell-Klein-Gordon and Maxwell-Dirac Systems in Highly to Slowly Oscillatory Regimes*. PhD thesis, Karlsruher Institut für Technologie (KIT), 2017.

[4] Patrick Krämer and Katharina Schratz. Efficient time integration of the maxwell–klein–gordon equation in the non-relativistic limit regime. *Journal of Computational and Applied Mathematics*, 316:247–259, 2017. Selected Papers from NUMDIFF-14.

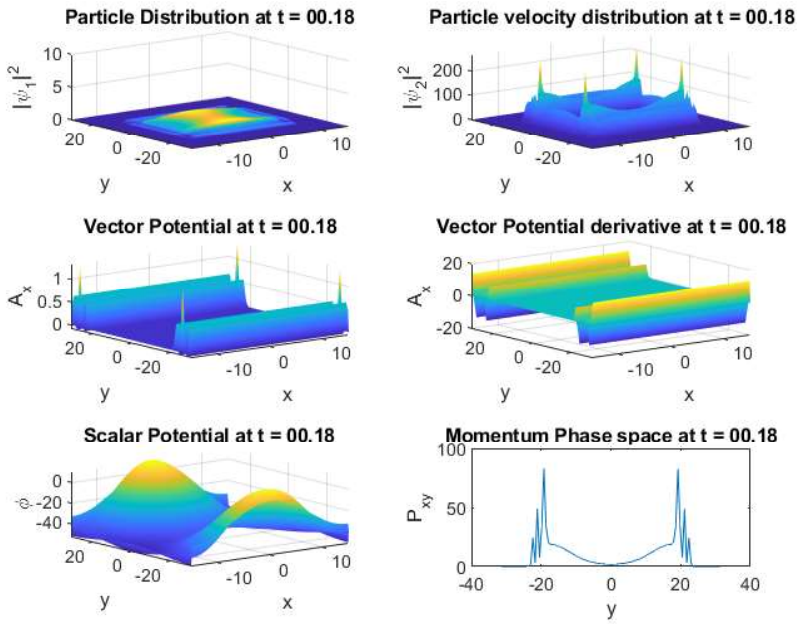

Figure 2: Results at $t = 0.18$ of simulation time with a time step of 0.015. The results show the solutions and their derivatives as well at a phase space slice down the center along the y axis.

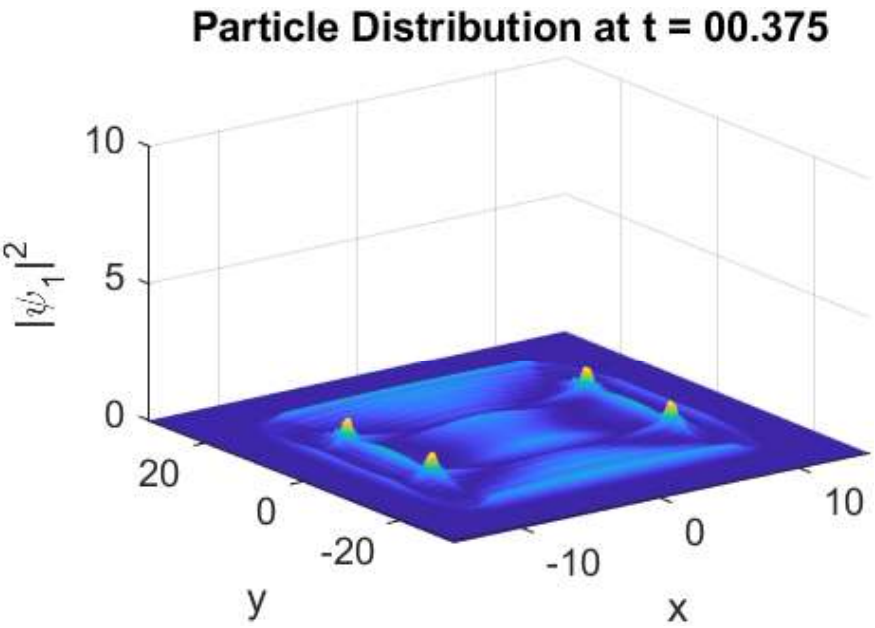

Figure 3: Results of the simulation at t = 0.375 where saddle points in the self-scalar potential begin to form.

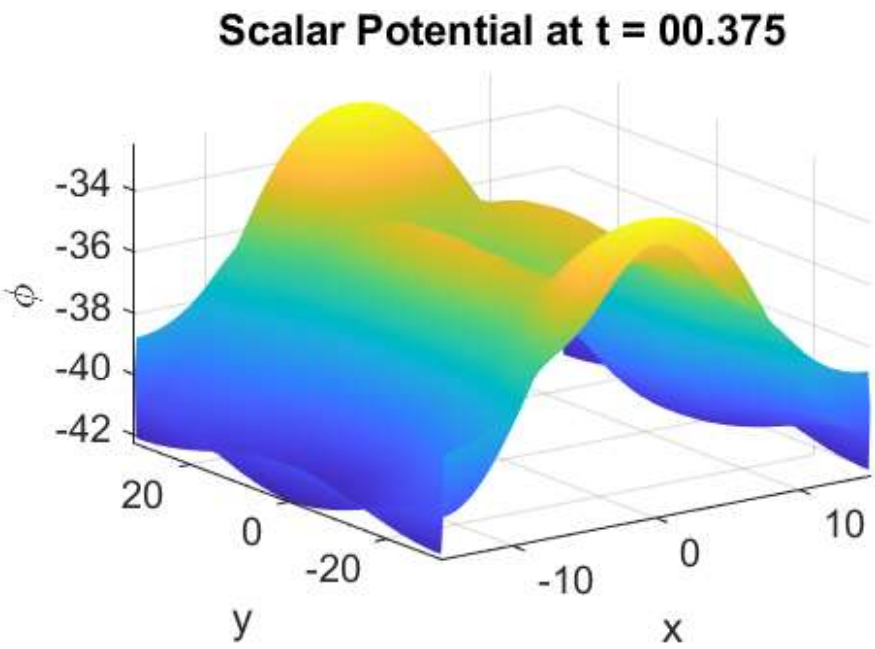

Figure 4: Saddle points in the potential energy due to the self-consistency of the particle distribution.

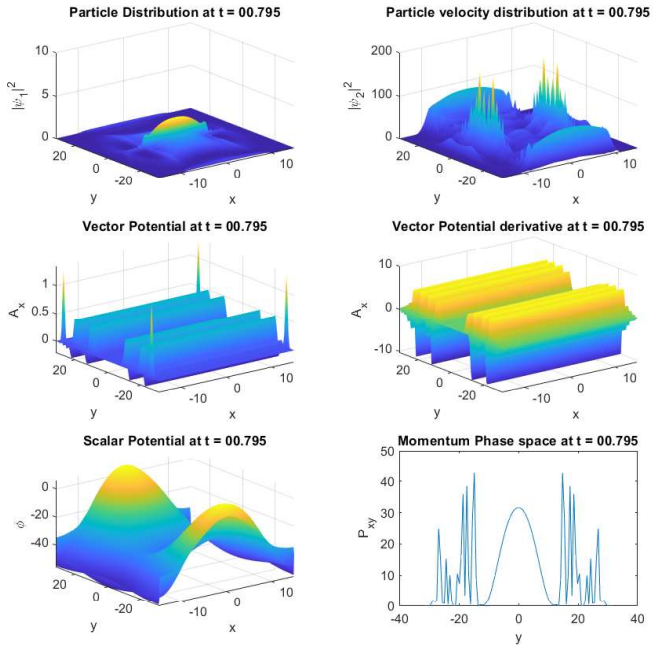

Figure 5: Simulation results showing a spike in particle velocity following the wake of a CPEM wave vector potential. The phase space momentum plot shows a spiking that is reminiscent of the 1D results of [2] where the momentum has a smooth middle part with a sharp and jagged outer part due to the nonlinearity of the system.

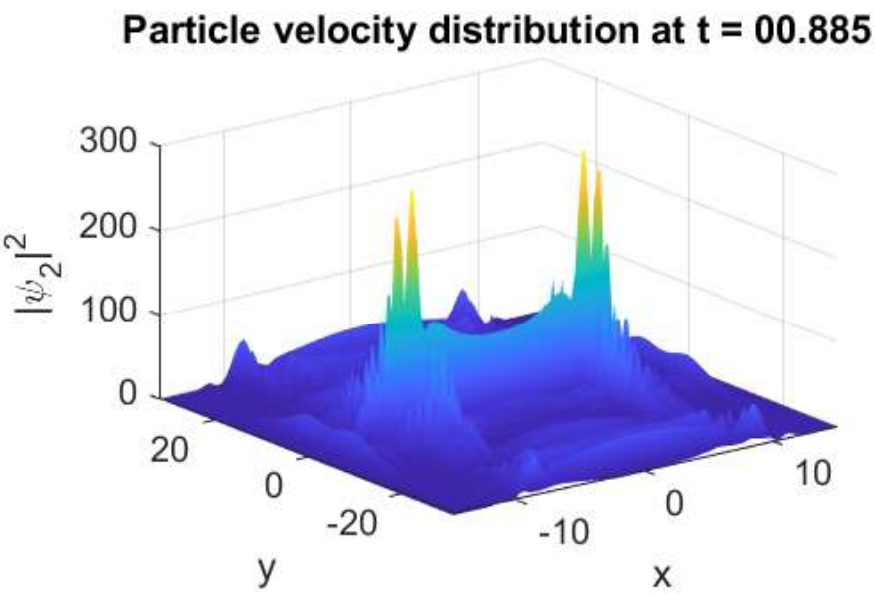

Figure 6: Particle velocity distribution showing nearly the maximum velocity the particles reach before slowing down again.